Y/DZ-3207

Deformation Behavior and Texture Evolution of Steel Alloys under Axial-Torsional Loading

Akawut Siriruk, Matthew Kant, Dayakar Penumadu
University of Tennessee, Knoxville, TN

Elena Garlea
Y-12 National Security Complex

Sven Vogel
Los Alamos National Laboratory, Los Alamos, NM

June 2011

Prepared by the
Y-12 National Security Complex
P.O. Box 2009, Oak Ridge, Tennessee 37831-8169
managed by
Babcock & Wilcox Technical Services Y-12, LLC
for the
U.S. DEPARTMENT OF ENERGY
under contract DE-AC05-00OR22800

Deformation Behavior and Texture Evolution of Steel Alloys Under Axial-Torsional Loading

Akawut Siriruk[1], Matthew Kant[1], Dayakar Penumadu[1], Elena Garlea[2], Sven Vogel[3]

[1]University of Tennessee, Knoxville, TN
[2]Y-12 National Security Complex, Oak Ridge, TN
[3]Los Alamos National Lab, Los Alamos, NM

Using hollow cylinder samples with suitable geometry obtained from round bar stock, the deformation behavior of bcc Fe based 12L14 steel alloy is evaluated under multi-axial conditions. A stacked strain gage rosette and extensometer mounted on the cylindrical surface at the mid height of the specimen provided strain tensor as a function of applied stress for pure tensile and torsion tests prior to yielding. This study examines elastic and yield behavior and effects of these with respect to texture evolution. Hollow cylinder specimen geometry (tubes) with small wall thickness and relatively (to its thickness) large inner diameter is used. The variation of observed yield surface in deviatoric plane and the effect on mode of deformation (tension versus torsion versus its combination) on stress-strain behavior is discussed. Bulk texture was studied using neutron time-of-flight diffractometer at High-Pressure-Preferred Orientation (HIPPO) - Los Alamos Neutron Science Center (LANSCE) instrument and the evolution of texture and related anisotropy for pure tension versus torsion are also included.

INTRODUCTION

The pre-yield, hardening/softening, and failure behavior of bcc alloys can be affected by such factors as the applied stress/strain path, loading type, specimen microstructure and its anisotropy. Pure tensile and torsion tests simulate the stress/strain conditions corresponding to commonly occurring loading conditions for many structural materials. Although failure of alloys in tension has been extensively studied in the past, there is limited experimental data associated with multi axial stress-strain behavior of structural alloys that involves direct application of tension, torsion, and its controlled combination. It is important to understand how different loading paths affect the pre-yield and post yield behavior in three dimensions for modeling realistic constitutive models and solve boundary value problems, for example using Finite Element Method (FEM). In addition, there is limited work on detailed bulk texture characterization using neutron techniques in general for evaluating the texture evolution under torsion and combined tension-torsion loading.

Using an axial-torsional servo-hydraulic testing system, one can perform a complete set of stress paths to study three dimensional mechanical behavior using pure tension to pure torsion and their combination for simulating loading paths that involve fixed principal stress rotation. Thus, it is possible to fix the angle of major principal stress throughout a test and probe directional dependency of elastic and plastic properties such as shear modulus and yield stress and study the effect on crystallographic texture. To evaluate anisotropy, one performs tensile tests on samples obtained from different directions, however, this only provides the effect of texture on tensile yield stress, but the true shearing mode deformation is only possible by applying pure torsion on

tubes, rods, or prismatic sections. The effect of stress path (torsion versus tension or its combination) on the stress-strain behavior and the potential anisotopic state of yield surface can be obtained using procedures developed by Han and Penumadu [1]. The texture measurements and its evolution as a function of loading path will also fill a critical intellectual gap in the literature.

It is known that metallic materials exhibit variance in yield stress as a function of multi-axial loading (for example: tensile versus torsion). Guest could be considered one of the first to study elastic limits for multi-axially stressed metals, using thin tubes of steel, iron, and copper subjected to torsion, torsion with tension, tension, internal pressure with tension, and solely internal pressure [2-4]. Guest used the same sample to perform different stress path tests in this loading scheme, which caused his yield points to be subsequently higher upon reloading and his stress ratios, failure in shear to tension, to be ambiguous. Such an experimental approach also has the limitation of uncoupling the combined effect of texture and loading path. In general, his observations lead him to believe that the occurrence of plastic strain had little impact from the intermediate principal stress but was determined by the absolute value of a principal shear stress reaching a critical value [5]. Yu provides a comprehensive summary of past research that attempted three dimensional testing, providing a summary on materials evaluated, experimentally measured ratio of yield stress in shear to tension, and suitability of yield criteria considering the yield surfaces proposed by von Mises, Tresca, and the one based on Twin shear [6]. It shows that the discrepancies among different experiments and different materials are large and results do not agree with established yield criteria and no general conclusions can be inferred on suitability of a given yield criteria. Therefore, it is very important to choose a reasonable yield criterion experimentally, even for simple slip plane systems, as the yield behavior is largely controlled by its initial and evolving microstructure, processing and environmental conditions. Up to now it is still a problem to find a unified yield criterion that can be applicable to more than one kind of material, even when processed identically. Texture is largely ignored due to a lack of reliable measurement techniques in the past such as neutron scattering methods to yield bulk texture.

MATERIALS AND TESTING SYSTEM

Mechanical Testing System

A highly sensitive biaxial servo-hydraulic MTS mechanical testing system with a full-scale capacity of 25 kN axial force and 250 N-m torque, shown in Fig. 1a, was used to perform mechanical testing, applying tension and torsion simultaneously. An axial extensometer in Fig. 1b was used to record the on specimen axial strains from the deforming sample. The axial force obtained from the biaxial MTS system was also verified by comparing with a uniaxial tensile system having a 50 kN external load cell. The flat steel alloy samples were evaluated in tension using two different MTS servo-hydraulic testing systems (a 25 kN biaxial system as shown below and 100 kN axial MTS system) and results showed very high repeatability in Figure 2a. Moreover, a custom made Universal Testing Machine (UTM) that used electrical axial and torsional actuators developed by the senior author at the University of Tennessee in Figure 2b was also used to evaluate the accuracy of the biaxial MTS system and provided very similar experiments stress-strain results. Thus, it was concluded that the use of biaxial testing system for

all experiments on 12L14 samples resulted in a highly accurate data. Because of the ease in implementing PID control to perform complex combined axial-torsional loading tests, results obtained using MTS servo-hydraulic system are included in this paper.

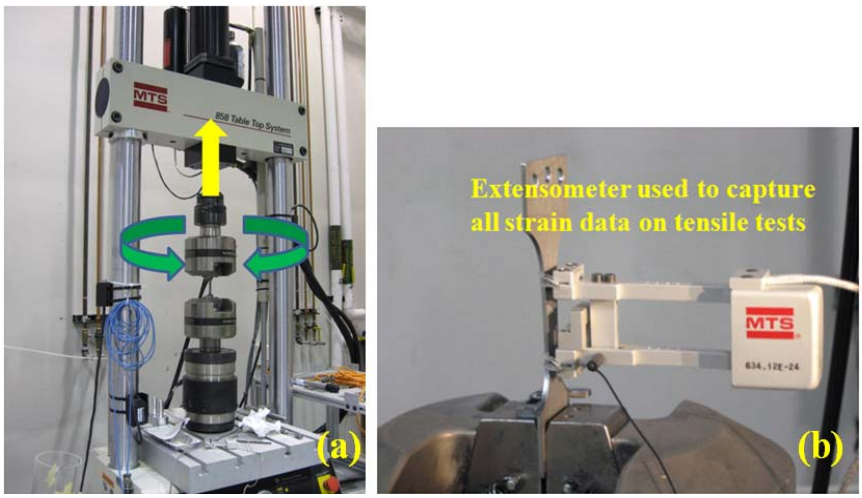

Fig. 1- (a) Biaxial testing system, (b) Tensile data captured by using an extensometer device

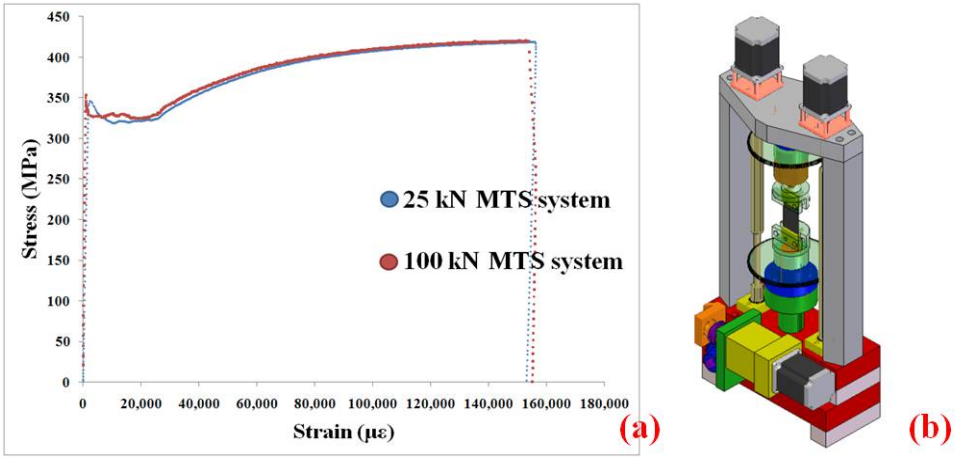

Fig. 2 – (a) Comparison of A36 steel alloy (flat samples) on two different testing systems, (b) Custom made testing system at University of Tennessee

Prior to beginning the experiments, the Proportional, Integral, Derivative (PID) control values were tuned to accurately control biaxial tests used for this work [7]. To have a precise control on variables, the optimal values of PID terms are needed so that the error between input and output are minimal and the output is very stable throughout the test. It is important to note the PID values also depend on the material type and geometry. Thus, a number of dummy samples were used to perform the required tuning. Successful PID parameters were developed with optimally tuned gain parameters to maintain a constant ratio of tensile stress increment to shear stress increment, resulting in a fixed value of principal stress rotation angle (β) throughout a given test.

A stacked strain gage rosette was used to evaluate the multi-axial strain state as a function of applied stress in the elastic regime very precisely. The rosette was mounted at the mid height of the specimen, and the complete state of strain tensor was obtained from the response of the three strain gages as a function of applied stresses. Figure 3 shows the 0°/±45° rosette strain gage attached on 12L14 steel samples as configured for this study.

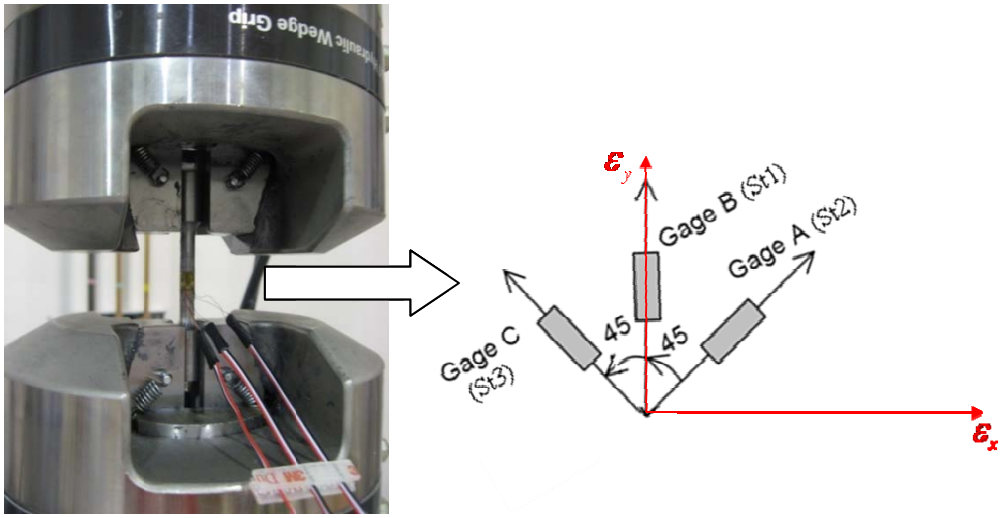

Fig. 3 - Experimental set up for a hollow cylinder and a schematic of 0°/ ±45° rosette strain gage.

12L14 Steel Alloy Materials

The 12L14 steel alloy hollow cylinder specimens used in this work have the ideal geometry for torsion test specimens. For such tests, the sample with hollow cylinder cross-section and thin wall thickness ensures the radial variation of the shear stress in the cross-section to be small, simplifying the study of three-dimensional constitutive behavior. A picture of the hollow cylinder specimen with dimensions used in our study is shown in Fig. 4a and 4b. Over the gage length, the outer diameter is 6.0 mm and the wall thickness is 1.5 mm. Standard composition of 12L14 steel is given in Table 1. A gage length of 32.5 mm satisfies Venant Principle, preventing unwanted grip effects on expected stress state [8].

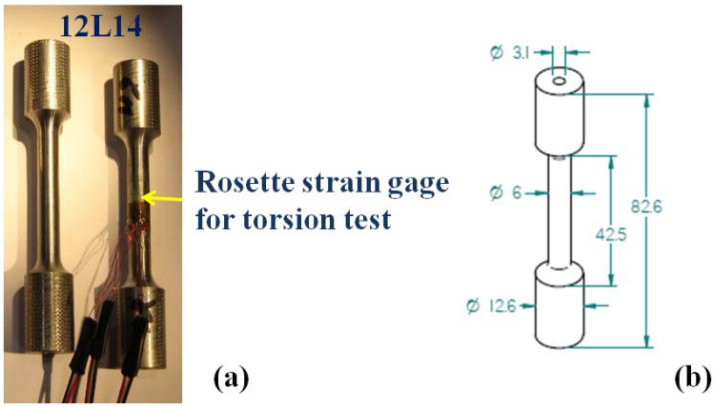

Fig. 4 - (a) 12L14 steel hollow cylinder with rosette strain gage, (b) schematic with dimension of 12L14 hollow cylinder sample

Table 1 - Typical Chemical Composition of 12L14 steel

AISI Number	Chemical compositions (%)				
	C max	Mn	P	S	Pb
12L14	0.15	0.85-1.15	0.04-0.09	0.26-0.35	0.15-0.35

EXPERIMENTAL SETUP

Pure Tensile and Torsion Test

All tensile tests were performed as per ASTM E8/E8M [9]. The 12L14 hollow cylinder samples were subjected to pure tension at a strain rate of 0.2 mm/min and a maximum of 1.5 mm displacement. An extensometer was attached at the mid height to obtain on specimen strain data in all experiments. Equation 1 is used to determine average initial values of elastic modulus, *E*.

$$E = \frac{\Delta\sigma}{\Delta\varepsilon} \qquad \text{(eq. 1)}$$

Pure torsion tests were performed at the rate of 3 deg/min and under zero axial stress, $\sigma = 0$. The hollow cylinder specimens were subjected to 15 degrees of maximum rotation. A Strain gage rosette was used to obtain on specimen shear strain data (γ). The determination of *G* was calculated from Equation 2

$$G = \frac{\Delta\tau}{\Delta\gamma} \qquad \text{(eq. 2)}$$

Combined Tension-Torsion Test

Different loading paths corresponding to a fixed principal stress rotation angle (β) are used to investigate the effect of principal stress rotation.

$$k = \Delta\tau/\Delta\sigma = 1/2 \tan (2\ \beta) \quad \text{(eq. 3)}$$

where $\Delta\tau$ = the change of shear stress generated by the torque applied on sample.
$\Delta\sigma$ = the change of axial stress generated by the displacement control.
k = constant ratio of axial and shear stress change

This fixed value of *k* was used to implement real-time PID control to maintain the changes of both axial and shear stress increments constant time throughout the test.

The authors chose to use octahedral plane for displaying the effects of stress path and the state of stress associated with failure as this plane is invariant. On a given octahedral plane, each data point has an identical mean stress. The shear stress and strain on the octahedral plane can be computed as [10]

$$\tau_{oct} = \frac{1}{3}\sqrt{(\sigma_1 - \sigma_2)^2 + (\sigma_2 - \sigma_3)^2 + (\sigma_3 - \sigma_1)^2} \quad \text{(eq. 4)}$$

$$\gamma_{oct} = \frac{2}{3}\sqrt{(\varepsilon_1 - \varepsilon_2)^2 + (\varepsilon_2 - \varepsilon_3)^2 + (\varepsilon_3 - \varepsilon_1)^2} \quad \text{(eq. 5)}$$

Where τ_{oct} – octahedral shear stress
γ_{oct} – octahedral shear strain
σ_1, ε_1 – principal stress and strain in direction 1
σ_2, ε_2– principal stress and strain in direction 2
σ_3, ε_3 – principal stress and strain in direction 3

RESULTS AND DISCUSSIONS

Figure 5 shows the typical stress-strain curves behavior of a tensile test for 12L14 hollow cylinder samples. The Young's modulus from initial slope was determined to be 200 GPa. The average yield stress was 600 MPa from 0.2% offset. Figures 6 and 7 shows typical average shear stress-strain behavior of a 12L14 steel specimen subjected to a torsional test. The torsion measurements results on 12L14 hollow cylinder sample based on the rosette strain gage which represent the maximum shear strain yielded a shear modus of 79 GPa and the average yield stress was 400 MPa in Figure 6 with 0.2% offset. With the same result, Fig. 7 showed the average shear stress and strain. An expression for the average shear stress and shear strain used for this interpretation can be seen in equations 7 and 8 [11].

$$\tau_{\max} = \frac{2TR_o}{\pi(R_o^4 - R_i^4)} \quad \text{(eq. 6)}$$

$$\tau_{average} = \frac{3T}{2\pi(R_o^3 - R_i^3)} \quad \text{(eq. 7)}$$

$$\gamma_{average} = \frac{2\phi(R_o^3 - R_i^3)}{3H(R_o^2 - R_i^2)} \quad \text{(eq. 8)}$$

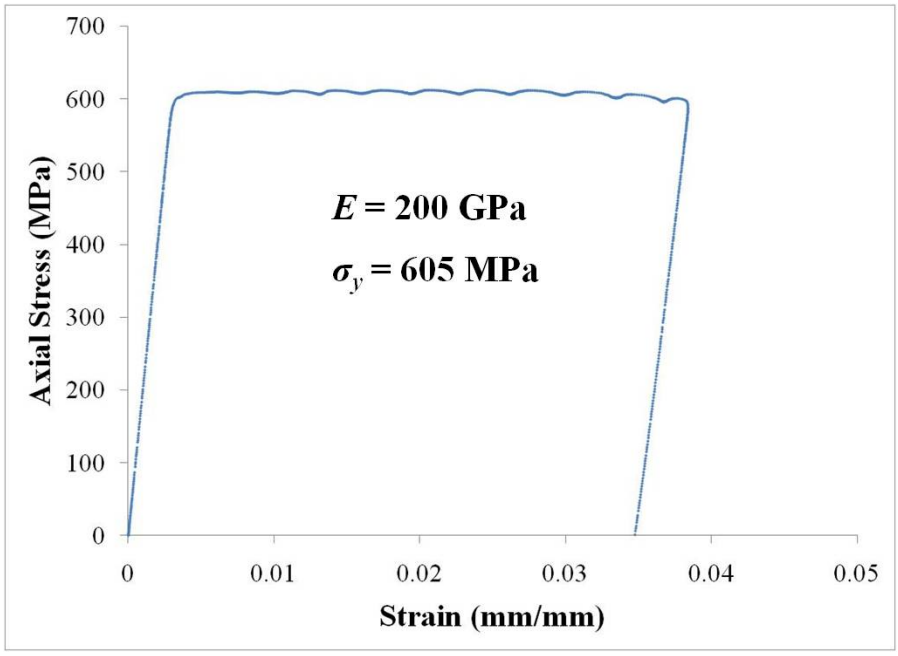

Fig. 5 - Typical stress-strain data of 12L14 hollow cylinder for the tensile test.

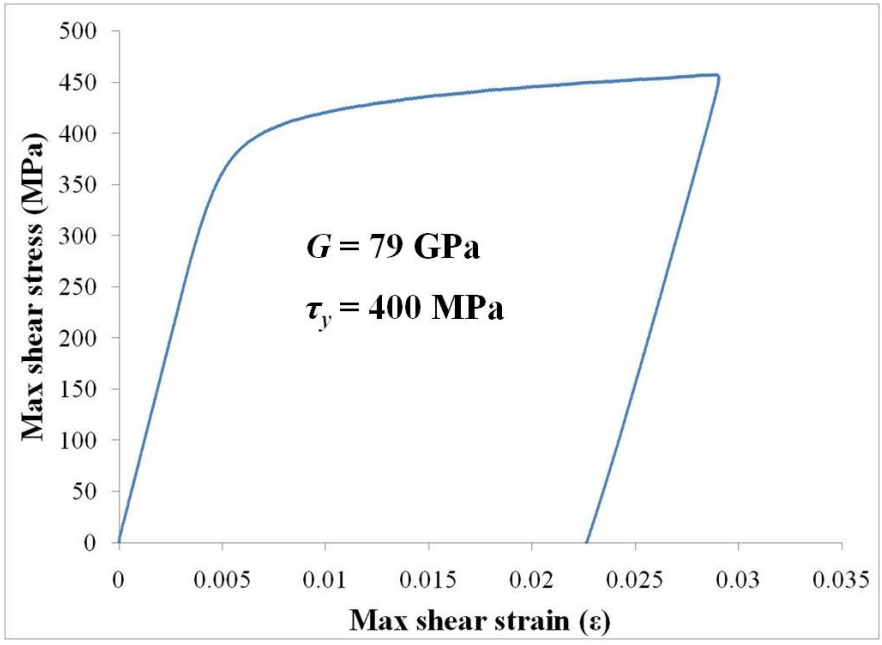

Fig. 6 - Typical maximum shear stress-strain data of 12L14 hollow cylinder for the torsion test.

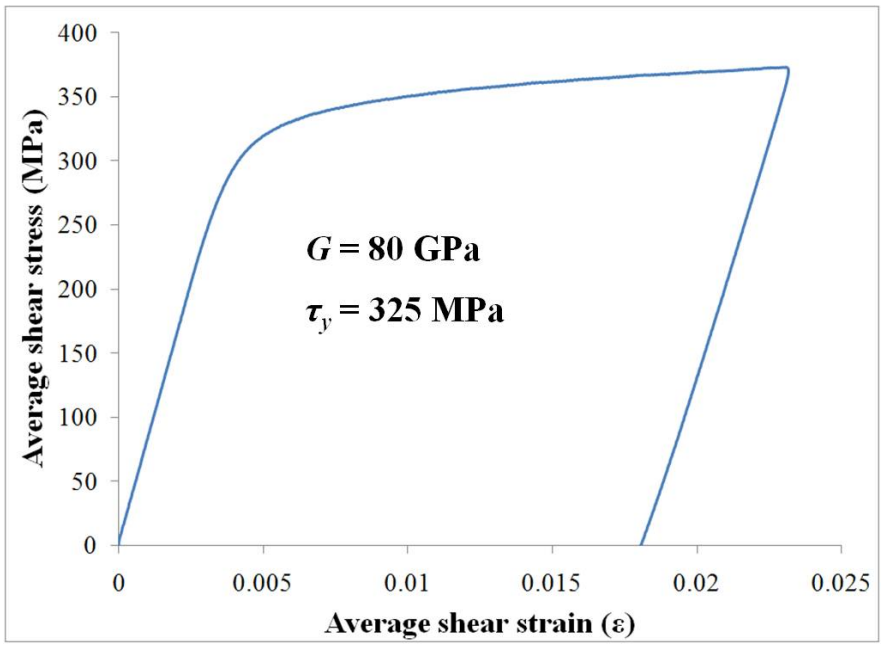

Fig. 7 - Typical average shear stress-strain data of 12L14 hollow cylinder for the torsion test.

12L14 samples were evaluated at given principal stress rotation with β values of 0 (pure tension), 15, 30 and 45 degree (pure torsion). As a result of successful PID tuning, both deformation and bi-axial load control procedures were optimized in the developed algorithm to obtain the accurate results. Figures 8 and 9 shows the constant value of the principal stress rotation angle on a 12L14 hollow cylinder specimen by keeping the same ratio of shear stress and axial stress increments throughout. The average value of the measured rotation angle throughout the test was 15.2 and 29.6 degree indicating a very good control of the testing system and procedure. Figures 8 and 9 verify true β control testing, showing constant ratio both during pre-yield and post yield stages of the test. Because a rosette strain gage was used to record on specimen axial and shear strains on the sample, combined tension-torsion deformation may cause inaccurate post yield axial strain data. Thus, it is important note that within the elastic range various β values showed no effects on Young's and shear modulus as in Fig. 10.

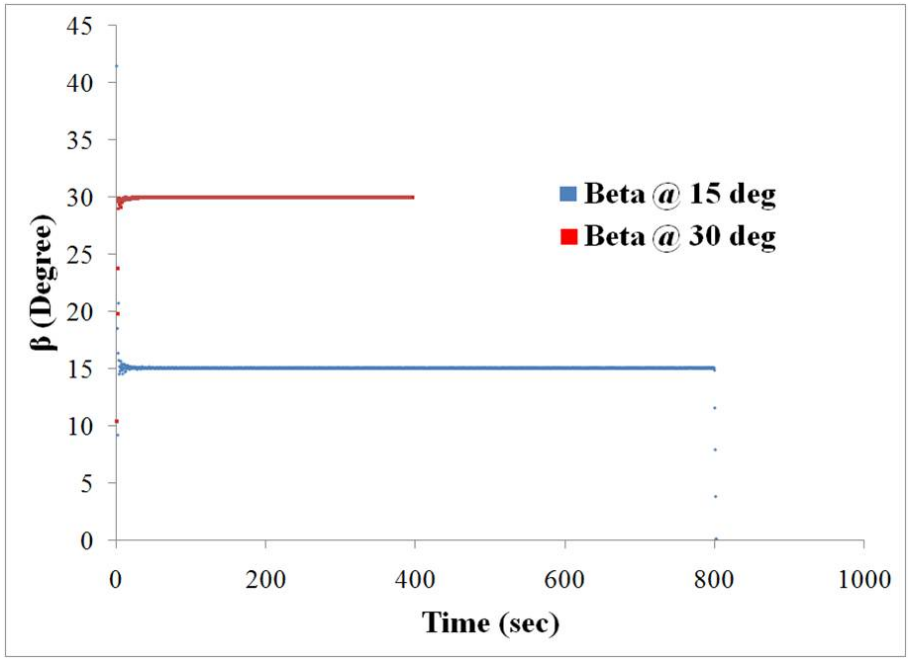

Fig. 8 - Variation of principal stress rotation angle at β = 15 and 30 degree on 12L14 steel hollow cylinder sample.

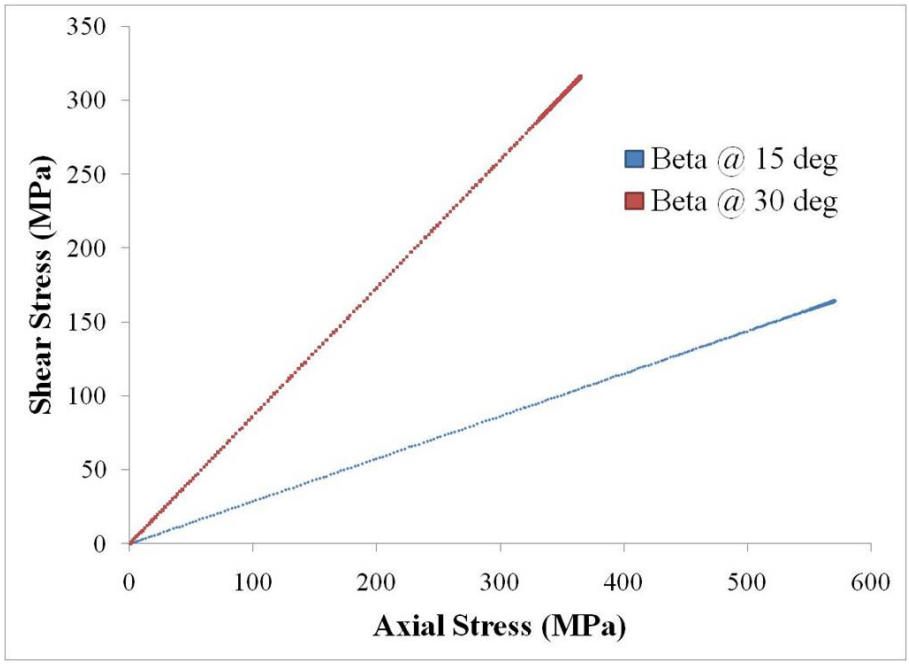

Fig. 9 - Typical test result of shear stress vs. axial stress at β = 15 and 30 degree.

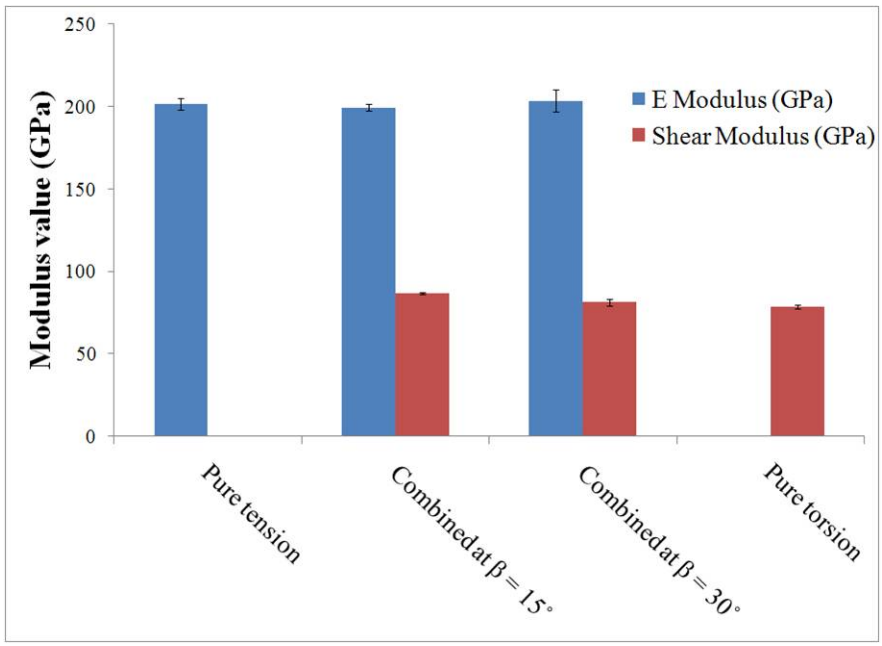

Fig. 10 - Comparison of Young's and shear modulus of 12L14 hollow cylinder at given β.

Limitations arise in the determination of axial and shear strain under plastic deformation with strain gage or extensometer measurements during combined bi-axially loading. Consequently, the global LDVT data become the more accurate source for axial and shear strain, but a calibration factor must be included to account for compliance effects. These calibrations were determined by comparing LVDT axial and shear strain during linear material response with extensometer strain in tension and strain gage in torsion. The updated LVDT strains have been referred to as "corrected strain" in the work presented.

In general yield condition occurs at the initiation of inelastic material behavior when material yields. The strong effect of multi-axial loading on stress-strain behavior can be seen for β = 0, 15, 30, 45 degree in Fig. 11. It can be seen that principal stress rotation has a strong influence on both the slope of stress-strain curve, state of stress corresponding to yield, and post-yield behavior in terms of associated plasticity behavior. A consistent trend of stress-strain curve was observed as β increased.

Generalized yield criteria for 12L14 hollow cylinder samples was obtained by plotting the state of stress at yield for varying fixed β tests in three dimensional stress space. Using suitable coordinate and stress-strain transformation procedure explained in Barbero [13], material yielding behavior could be represented in a unified frame work considering the measurements that include multi-axial stress states. Figure 12 demonstrates that 12L14 steel followed Von Mises failure criteria for β from 0 – 30 degree, but overestimates yield behavior at 45 degrees assuming a 0.2% offset yield law. The shape of the Von Mises yield surface in deviatoric space is a circle. For isotropic materials all angles, 0 to 360, degrees are not needed, as the information would be redundant from sample symmetry. Hence, the rest can be obtained by mirroring the data points [10].

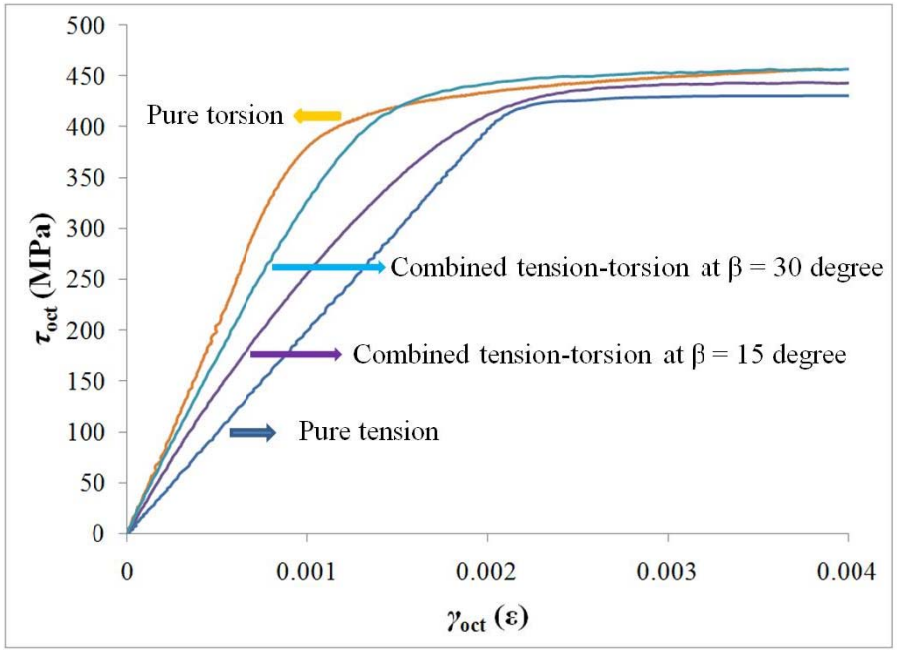

Fig. 11 - Multi axial loading on stress-strain behavior of 12L14 hollow cylinder.

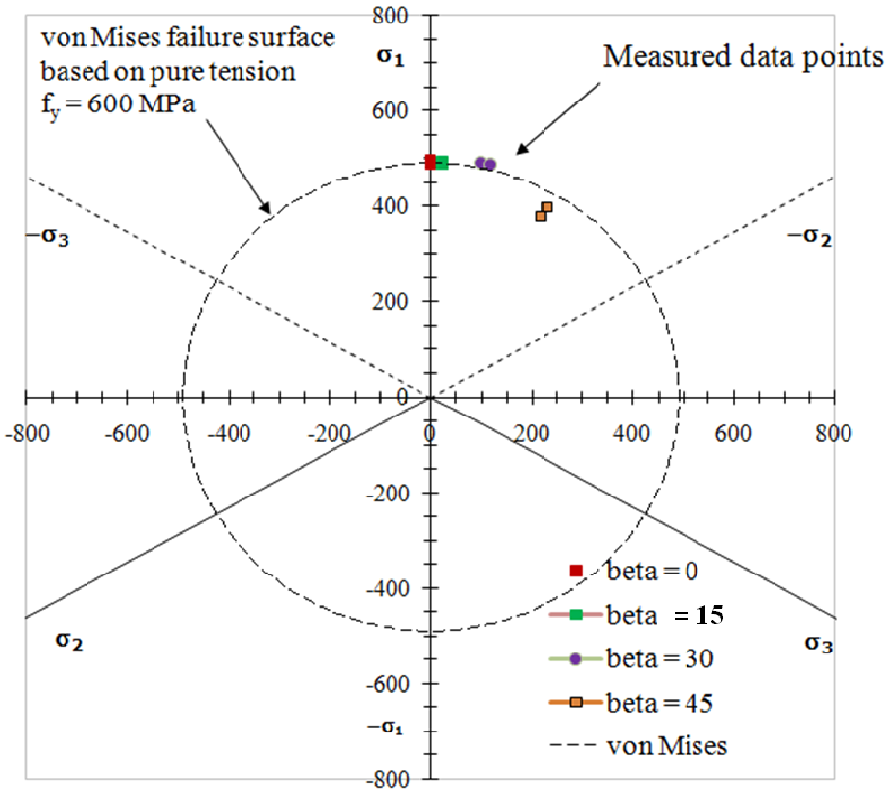

Fig. 12 - Yield surface criteria of 12L14 hollow cylinder sample compared to Von Mises failure surface based on yield stress of 600 MPa.

Texture Measurements

Texture measurements on stressed and unstressed steels were made at LANSCE (Los Alamos Neutron Science Center) using the time of flight (TOF) HIPPO (High-Pressure-Preferred Orientation) diffractometer [14]. The purpose was to study the texture evolution induced from deformations for axial-torsional testing that involved rotation of major principal stress with respect to hollow cylinder axis. One of the main advantages of neutron as opposed to x-ray diffraction is the ability to study large sample volumes, which makes them ideal for texture measurements where bulk rather than surface effects are of particular interest. Three samples were studied using neutron diffractometer that corresponded to an unstressed sample (for reference or initial texture), one sample that was subjected to strains well beyond yield in pure tension, and one sample subjected to strains well beyond yield in pure torsion. Both samples strained well beyond yield in tension or torsion had the same octahedral shear strain prior to unloading to zero stress state. The alignment was setup such that the 10mm diameter beam hit the samples the center of their gage region. The 40, 90, and 150 degree detector banks of the HIPPO instrument and sample were oriented as shown in Fig. 13. Excellent pole figure coverage was achieved with 3 sample rotations, as demonstrated in Fig. 15 for two different pole figure orientations, the sample rotation axis in the center of the pole figure and the neutron beam in the center of the pole figure. The hollow cylinder samples were oriented in HIPPO such that the tensile axis and the sample rotation axis were the same seen as the ZZ axis in Fig. 14. A computer program, Materials Analysis Using Diffraction (MAUD) was used to calculate the textures from the TOF spectra using the Rietveld method. For details, refer to procedures developed to extract material textures from TOF spectra by Wenk, Lutterotti, and Vogel [15]. A more complete description of the coordinate system in the MAUD software relative to the HIPPO instrument has been presented by Kocks et al. [15].

Texture represented using Pole figures for three hkls for BCC 12L14 steel samples is shown in Figs. 15, 16, and 17. Rows A, B, and C represent no deformation, sample subjected to tension, and sample subjected to torsion, respectively. For the 12L14 tubular samples neither tension nor torsion made any noticeable difference the preferred texture orientation shown in Figs. 16 and 17 for the two pole figure orientations mentioned. Although, texture formation from torsion is not commonly significant, tensile deformation does commonly produce a texture [16]. This indicates that sample geometry or sample processing, specifically initial conditions of the material, and is critical to understanding the development of texture under large plastic strains. The lack of texture evolution under stress could also be a result of strain localizations during deformation. Only a small 10mm beam diameter window was irradiated, and this could have easily missed a high strain region where texture evolution would have been expected to occur.

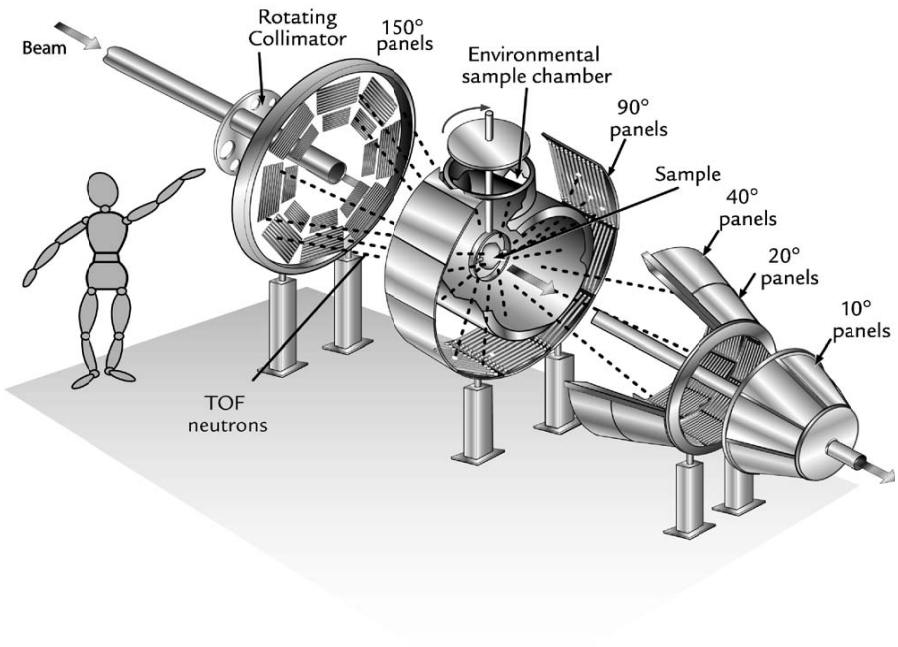

Fig. 13 - Drawing of HIPPO diffractometer at LANSCE [14]

Fig. 14 - Sample axis reference for pole figure orientation

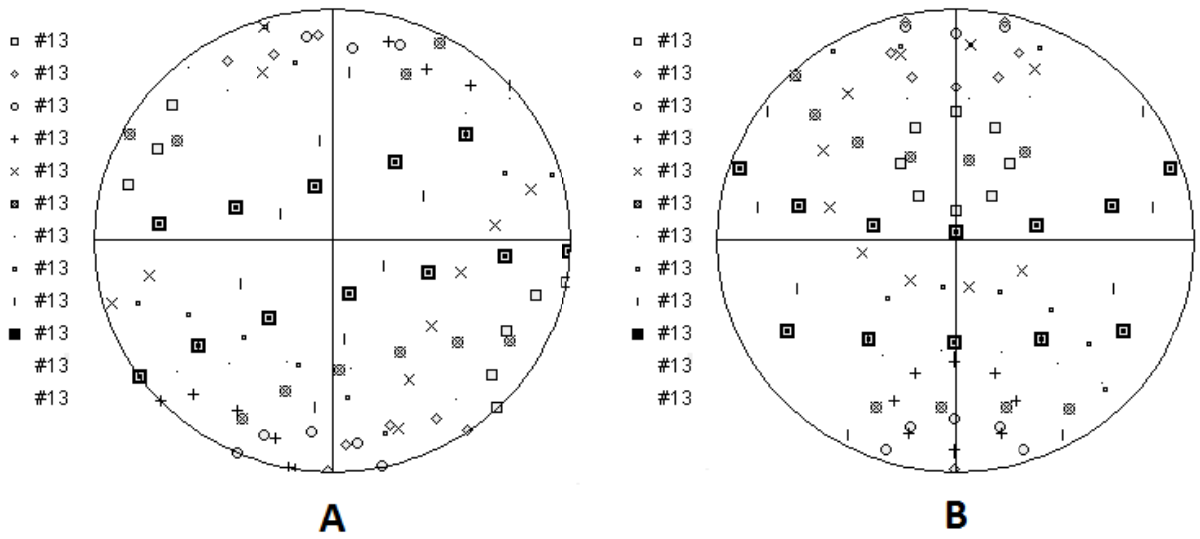

Fig. 15 - Pole figure coverage for 12L14 unstressed sample. The symbols represent the 12 spectra, 4 sample positions and 3 detector banks. A) Beam is center of pole figure. B) Beam in plan of pole figure.

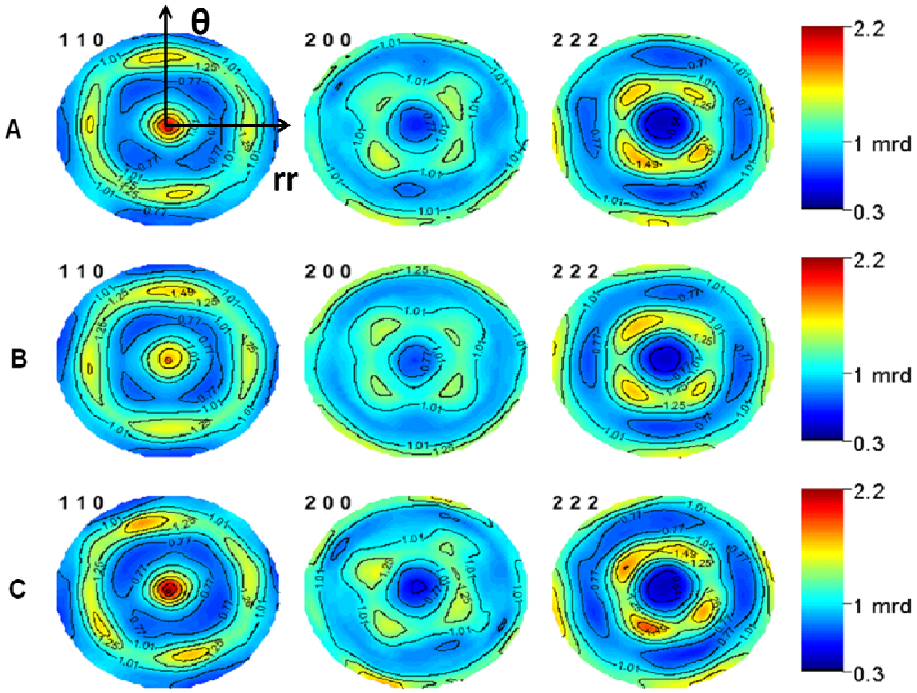

Fig. 16 – Pole Figures 12L14 steel with ZZ axis in center A) Unstressed B) Tension C) Torsion

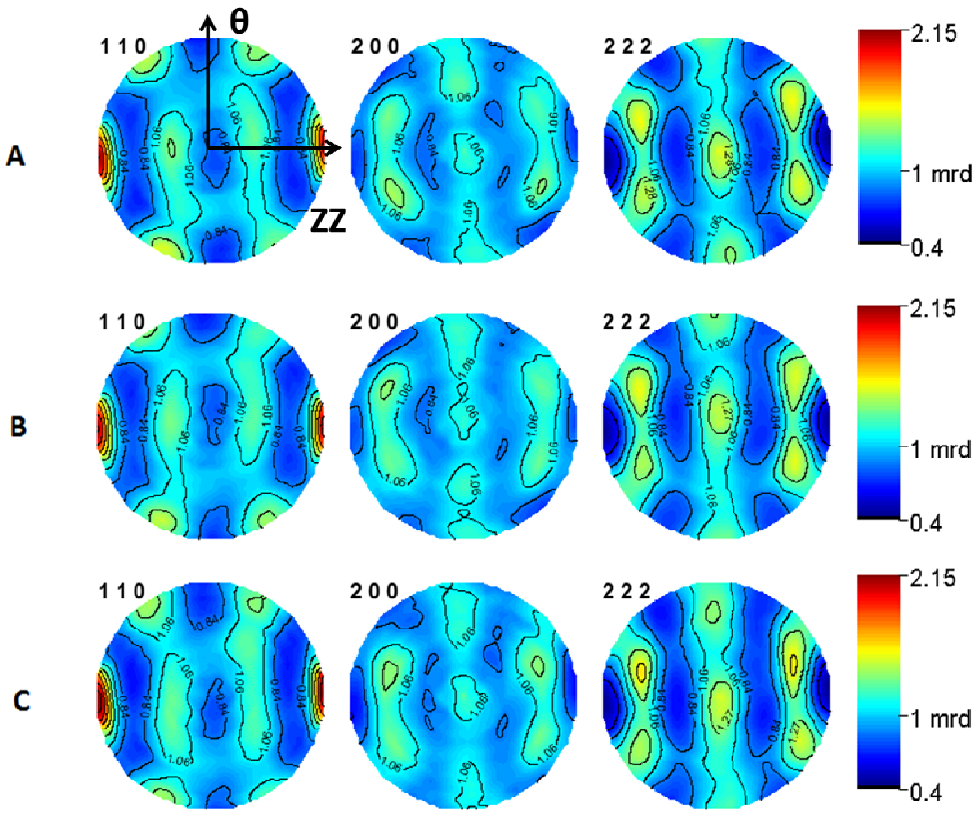

Fig. 17 – Pole Figures 12L14 steel with beam line in center A) Unstressed B) Tension C) Torsion

CONCLUDING REMARKS

Combined tension and torsion testing with variable stress paths were performed on hollow 12L14 steel cylinders. It was shown that for Beta from 0-30 the Von Mises yield criteria predicted failure well, but over predicts for Beta of 45 or pure torsion case. Bulk texture measurements using TOF neutron diffraction were performed at the Lujan Neutron Scattering Center at Los Alamos National Labs on unstressed, pure tension, and pure torsion samples. The stressed samples were deformed well beyond yield, yet no texture change was noticed from the pole figures. This could indicate that sample geometry and processing are more important factors in predicting tension or torsion related texture evolution. Additionally, strain localizations in the gage region of the sample could have been missed in the irradiated volume, leaving the texture changes undetected.

ACKNOWLEDGEMENTS

References

[1] Han, L. and Penumadu, D., 2006, "Strain Localization in Combined Axial-Torsional Testing," J. Engrg. Mech., 132(5), pp. 555-564.

[2] Michno, M.J. and Findley, W.N., 1976, "An historical perspective of yield surface investigations for metals," International Journal of Non-Linear Mechanics, 11(1), pp. 59-82.

[3] Guest, J.J., 1900, "V. On the strength of ductile materials under combined stress," Philosophical Magazine Series 5, 50(302), pp. 69-132.

[4] Nadai, A., 1950, "Theory of Flow and Fracture of Solids," New York: McGraw-Hill.

[5] Taylor, G.I. and Quinney, H., 1932, "The Plastic Distortion of Metal," Philosophical Transactions of the Royal Society of London. Series A, 230, pp. 323-362.

[6] Yu, M.-h., 2002, "Advances in strength theories for materials under complex stress state in the 20th Century," Applied Mechanics Reviews, 55(3), pp. 169-218.

[7] MTS manual

[8] Hartog, J. P. D., 1987, "Advanced Strength of Materials," Dover Publications.

[9] ASTM E8/E8M, "Standard Test Methods for Tension Testing of Metallic Materials," American Society for Testing and Materials.

[10] Chen, W., and Saleeb, A. F., 1994, "Constitutive Equations for Engineering Materials: Volume 2," Elsevier Publishing Company.

[11] Lee, D., Juang, C. H., Chen, J., Lin, H., and Shieh, W., 1999, "Stress paths and mechanical behavior of a sandstone in hollow cylinder tests." International Journal of Rock Mechanics and Mining Sciences, 36(7), pp. 857-870.

[12] Timoshenko, S. P., and Goodier, J., 1970, "Theory of Elasticity," McGraw Hill Higher Education.

[13] Barbero, E. J. (2010). *Introduction to Composite Materials Design, Second Edition*. CRC Press.

[14] Wenk, H.R., Lutterotti, L. and Vogel, S., 2003, "Texture analysis with the new HIPPO TOF diffractometer." Nuclear Instruments and Methods in Physics Research Section A: Accelerators, Spectrometers, Detectors and Associated Equipment, 515(3), pp. 575-588.

[15] Wenk, H.R., Lutterotti, L. and Vogel, S., 2010, "Rietvel texture analysis from TOF neutron diffraction data." JCPDS-ICDD, 25(3), pp. 283-296.

[16] Kocks, U. F., Tomé, C. N., Wenk, H.-R. 1998, "Texture and Anisotropy," Cambridge University Press.